Quasi-Hexagonal Ordered Arrays of FePt Nanoparticles Prepared by a Micellar Method *

QU Sheng(屈盛), ZHANG Xing-Wang(张兴旺)**, YIN Zhi-Gang(尹志岗), YOU Jing-Bi(游经碧), CHEN Nuo-Fu(陈诺夫)

Key Lab of Semiconductor Materials Science, Institute of Semiconductors, Chinese Academy of Sciences, Beijing 100083

(Received 26 August 2007)

Hexagonally ordered arrays of magnetic FePt nanoparticles on Si substrates are prepared by a self assembly of diblock copolymer PS-b-P2VP in toluene, a dip coating process and finally plasma treatment. The as-treated FePt nanoparticles are covered by an oxide layer that can be removed by a 40 s Ar^+ sputtering. The effects of the sequence of adding salts on the composition distribution are revealed by x-ray photoelectron spectroscopy measurements. No particle agglomeration is observed after 600° C annealing for the present ordered array of FePt nanoparticles, which exhibits advantages in patterning FePt nanoparticles by a micellar method. Moreover, magnetic properties of the annealed FePt nanoparticles at room temperature are investigated by a vibrating sample magnetometer.

PACS: 75.50.Bb, 81.05.Bx, 81.07.−b

FePt alloy is a great promising magnetic recording medium material for area density beyond 1 Tbit/in^2, because it has significantly high magnetocrystalline anisotropy energy density (6.6×10^7–10×10^7 erg/cm^3) to suppress superparamagnetism at particle size of several nanometres.[1−3] Various methods of synthesizing FePt-based nanomaterials have been developed, including vacuum deposition techniques[4−6] and solution-phase chemical procedures.[3,7−10] However, random nucleation and growth of nanoparticles by using vacuum deposition technique generally result in relatively large crystalline size and broad size distributions, which adversely affect their magnetic performance. In contrast with all the physical deposition processes, the advantages of the chemical solution methods are the high degree of uniformity in the grain size and position. Generally, the FePt nanoparticles synthesized by chemical methods are covered by the organic ligand shell to prevent particle aggregation during array formation on a substrate. However, the ligand shell is expected to influence the magnetic properties and can be converted to a carbonaceous coating around particles during the post annealing process.[3] Furthermore, it has been observed that annealing required for the formation of $L1_0$ phase FePt can lead to particle agglomeration[8,9] which results in increasing switching volumes and media noise.

A reverse micellar method is usually employed for reducing single element metal ions into metal particles.[11−15] Comparatively, few reports[16] fabricating FePt nanoparticles by the micellar method are available. In this study, we employ the diblock copolymer micellar method to synthesize quasi-hexagonal ordered arrays of FePt nanoparticles, and particle agglomeration can be avoided during the post-annealing. Furthermore, the effects of the sequence of adding salts on the composition are also investigated.

The micellar method[12,13] is based on the self-organization of the diblock copolymer poly(styrene)-block-poly(2-vinylpyridine)(PS-b-P2VP) in toluene. A [PS(1670)-*b*-P2VP(700)] diblock copolymer is dissolved in toluene resulting in the formation of inverse micelles. Metal salts ($FeCl_3$, H_2PtCl_6) were added to the solution and, while stirring continues, the metal salts were equally dispersed into the micellar cores (2VP unit) by proton transfer. To transfer the metal-salt-loaded micelles onto a substrate, a Si substrate is immersed into the solution and pulled out at a constant speed of 12 mm/min. In order to remove the polymer matrix, the array of micelles is subsequently exposed for 5–30 min to a 100 W oxygen and hydrogen plasma within an isotropic plasma etcher (TePla 300). To investigate the effect of the sequence of adding metal salts on the microstructure of metal nanoparticles, three batches of samples were prepared in this work. As to the first batch of sample (sample A), $FeCl_3$ was added into the solution and then the solution was stirred for three days, and finally H_2PtCl_6 was added. Within the second batch of sample (sample *B*), the sequence of adding metal salts was reversed, adding H_2PtCl_6 firstly, then stirring, and finally adding $FeCl_3$. In the case of the third batch of sample (sample C), both $FeCl_3$ and H_2PtCl_6 were added simultaneously into the solution. The stoichiometric ratio of $FeCl_3$:H_2PtCl_6:2VP=0.25:0.25:1 kept a constant in all three batches.

The scanning electron microscopy (SEM) images presented in this study all were taken with a high res-

*Supported by Hundred Talents Programme Chinese Academy of Sciences, National High-tech R&D Programme of China under Grant No 2006AA03Z306, and the National Natural Science Foundation of China under Grant No 50601025.

Email: xwzhang@semi.ac.cn

© 2007 Chinese Physical Society and IOP Publishing Ltd

olution SEM (HITACHI S-4800) working at 10 kV. X-ray photoelectron spectroscopy (XPS) measurements were performed using a MKII electron spectrometer with a Mg K_α X-ray source (1253.6 eV). Magnetic properties were measured at room temperature by a Lakeshore 7404 vibrating sample magnetometer (VSM).

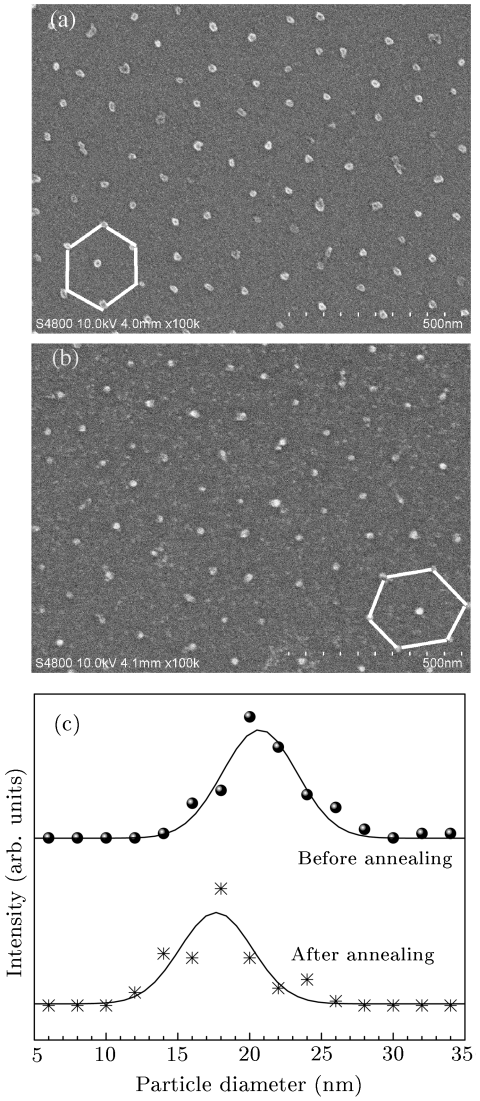


Fig. 1. HRSEM images of the ordered array of FePt nanoparticles (sample C) before (a) and after (b) 600°C annealing for 30 min; (c) size distribution of FePt nanoparticles corresponding to (a) and (b).

Figure 1(a) shows a typical SEM image of FePt nanoparticles on a Si substrate by a dip-coating process and oxygen plasma treatment for sample C. The surface exhibits a closely packed quasi-hexagonal structure, which is consistent with the surface morphology for the micelles loaded with single element metal salt.[12−14] The average particle size and the interparticle distance were found to be 21 and 100 nm in Fig. 1(a) (the height of nanoparticles is 9–12 nm as measured by atomic force microscopy). The formation of the hexagonal ordered arrays of FePt nanoparticles is described briefly in the following.[12] PS-b-P2VP diblock copolymers are dissolved in toluene resulting in the formation of inverse micelles, in which the core of the micelles consists of the hydrophilic P2VP blocks and the hydrophobic PS blocks form their shells. The core-forming block contains nitrogen atoms, and the free electron pair of N atoms is able to interact with inorganic salts and incorporates the precursor salt inside the micelles. By a dip coating process, a flat substrate can be covered homogeneously over the whole surface. During the slow evaporation of the solvent, liquid meniscus first forms between neighbouring particles, then well-ordered hexagonal arrays of metal-salt-load micelles were obtained in the assistance of capillary forces covering the whole surface of the substrate. Finally, the polymer matrix was removed by exposing the metal-salt-load micellar arrays to an appropriate plasma, and the lateral order of the resulting FePt nanoparticles is conserved.

To examine the remove of the polymer matrix and the chemical state, a series of XPS measurements were performed for the metal-salt-loaded micelles on Si after exposure to oxygen plasma for various time intervals. Figure 2(a) presents the C 1*s* binding energy region together with the N 1*s* core lines, both representing the elements to be removed by the plasma etching. A distinct N 1*s* signal and a strong C 1*s* signal are observed in the as-prepared sample (upper curve). After 30 min of plasma treatment, the N signal is found to completely vanish and the C intensity decreased remarkably. The residual C signal is attributed to adsorption of hydrocarbons due to sample transport in air. Thus, these spectra clearly indicate that the polymer matrix can be stepwise and finally completely removed through plasma treatment. Top two curves in Fig. 2(b) display Fe 2*p* and Pt 4*f* core-level spectra for the array of FePt-salt-loaded micelles before and after plasma treatment. Both Fe 2*p* and Pt 4*f* signals are weak in the as-prepared sample since the photoelectrons originating from the FePt-loaded core are strongly suppressed by the polymer matrix. The electron binding energies of Pt $4f_{7/2}$ and Fe $2p_{3/2}$ in metallic state are 71.2 eV and 706.8 eV, respectively.[17] The Pt $4f_{7/2}$ and Fe $2p_{3/2}$ peaks were observed at 74.8 eV and 711 eV for both the as-prepared and the plasma treatment sample in the present work, indicating Fe and Pt atoms in a highly oxidized state. The observed shifts of the binding energy for the as-prepared sample are attributed to the metal salt. Additionally, a weak shoulder peak at 71.5 eV attributed to metallic Pt was observed for the as-prepared sample because of the decomposition of the Pt salt under ambient conditions, and a similar result for Au-loaded micelles has been reported in Ref. [13]. To identify the origin of the chemical shift,

the XPS spectra were acquired for the plasma treatment sample after 2.0 keV Ar^+ ion sputtering for various time intervals, and the resulting spectra are also presented in Fig. 2(b). The Pt $4f_{7/2}$ and Fe $2p_{3/2}$ peaks shift to 72 eV and 707.2 eV for the all ion sputtering samples, which can be assigned to FePt alloy. Clearly, the plasma treatment causes simultaneously the complete removal of the polymer matrix, and the as-treated FePt nanoparticles were covered by a thin oxide layer that can be removed by a 40 s Ar^+ sputtering.

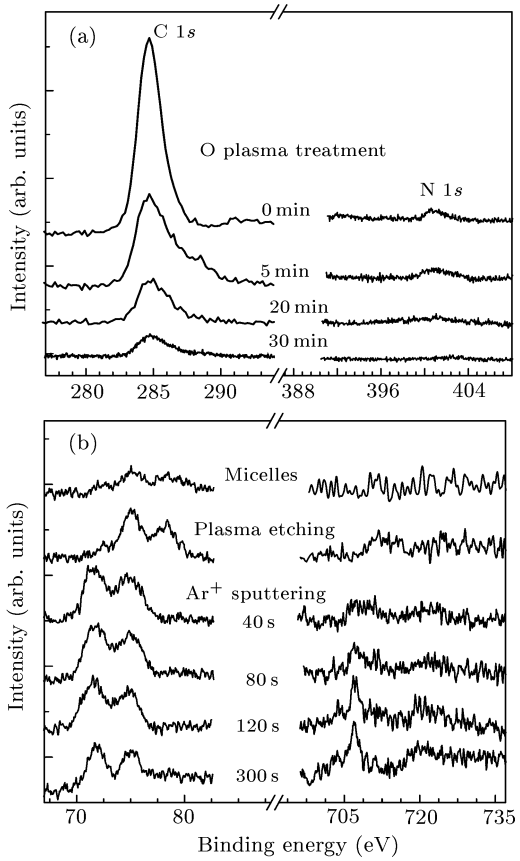


Fig. 2. (a) C 1*s* and N 1*s* core lines acquired from Fe and Pt salts loaded micelles on a Si substrate before and after exposure to the plasma for increasing times. (b) Fe 2*p* and Pt 4*f* core-level spectra for the array of FePt-salt-loaded micelles before (the top curve) and after plasma treatment (the second curve), followed by 2.0 keV Ar^+ ion sputtering for increasing times.

From Fig. 2(b) one can see that Fe and Pt XPS signals have different varieties with increasing sputtering time for the three samples. To study the effect of the sequence of adding salts on the composition distribution within the nanoparticles, we investigate the development of Pt $4f_{7/2}$ and Fe $2p_{3/2}$ core-level spectra as a function of the Ar^+ ion sputtering time for all three samples. The intensity ratio between Fe and Pt signals extracting from XPS results as a function of sputtering time is given in Fig. 3 for the three samples, in which the data is normalized to the plasma treatment sample (without Ar^+ sputtering). For different samples, corresponding to the different sequence of adding salt, the intensity ratio of Fe/Pt signal varies in completed different ways with Ar^+ sputtering time. For sample A (first adding Fe, then Pt), the intensity ratio between Fe and Pt signal increases with sputtering time, implying more Fe atoms situate at the core of FePt nanoparticles and while more Pt atoms locate at the particle shell. The opposite situation is observed for sample B with a reverse sequence of adding salt. On the other hand, simultaneously adding Fe and Pt salts leads to a uniform distribution of Fe and Pt as revealed by a constant intensity ratio for sample C. The results suggest that the salts added earlier are preferred to occupy the inner part of P2VP blocks, thus successively adding salt will be useful in synthesizing a core-shell structure for an immiscible system. While for a miscible system, e.g. Fe-Pt alloying particle, simultaneously adding Fe and Pt salts is favoured to obtain a uniform composition distribution.

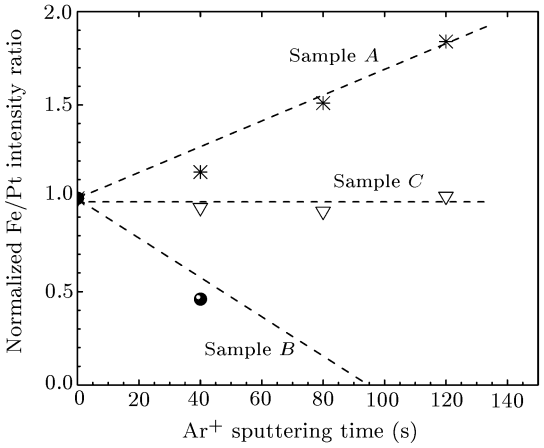


Fig. 3. Intensity ratio between Fe and Pt XPS signals as a function of Ar^+ sputtering time for the three samples. The dashed lines are only to guide the eyes.

A post-annealing is usually required to achieve the chemically ordered, high anisotropy ferromagnetic $L1_0$ phase, however, one serious side effect of the annealing is the deterioration of monodispersivity of the particles and loss particle positional order due to extensive particle aggregation.[8,9] To evaluate the stability of the present array of FePt nanoparticles, sample C was subjected to a 600°C annealing under 10^{-3} Pa for 30 min, and the corresponding high resolution SEM images are shown in Fig. 1(b). The particle arrangement exhibits a well hexagonal order in Fig. 1(b), as indicated by the hexagons in the images. More importantly, no evidence for particle agglomeration was observed after 600°C annealing, exhibiting an excellent stability against annealing for the array of FePt nanoparticles. Particle agglomeration was not observed even for FePt nanoparticles with the interparticle spacings of about 25 nm. With further increasing

total surface coverage of FePt particles required by a high storage density, the risk of getting agglomeration of the particles presumably goes up. Actually, in that case one can deposit in-situ a thin nonmagnetic layer (e.g. BN or C) to prevent from the particle agglomeration. Furthermore, the size distribution of the nanoparticles extracted from such images exhibits Gaussian characteristics, as shown in Fig. 1(c).

To investigate magnetic properties of FePt nanoparticles, the hysteresis loops of the 600°C annealed sample were measured by VSM. Figure 4 shows the in-plane M-H loop of sample C measured at room temperature, and the in-plane coercivity value is 80 Oe. The coercivity values of our samples are lower after annealing. This may be due to the surface oxidation of the FePt nanoparticles and/or the partial ordering of the annealed FePt nanoparticles. The oxidation of the FePt nanoparticles as confirmed by above XPS results leads to the reducing of the size of FePt nanoparticles and finally the lower coercivity. On the other hand, the partial ordering of FePt nanoparticles may also be responsible for the lower coercivity as reported in Ref. [18], in which they observed a coercivity value of 100–110 Oe at 300 K for the heat-treated FePt nanoparticles prepared by the high-temperature solution method. Moreover, the remanent magnetization is found significantly lower than $0.5M_s$, which also indicates that only a minority of nanoparticles has been fully transformed after 600°C annealing.

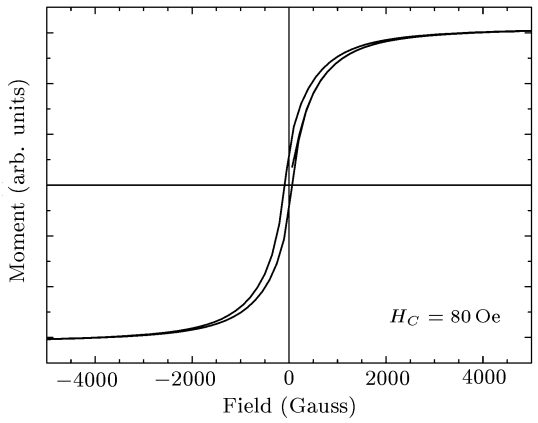


Fig. 4. In-plane *M–H* loop of FePt nanoparticles (sample C) measured at room temperature by using a VSM.

It is worth mentioning that the particle sizes (1–30 nm) and inter-particle distances (25–200 nm) can be adjusted by the amount of metal salt added to the micellar solution, the dipping velocity and the length of the involved copolymer using this technique,[13] which is an important advantage in fabricating ultrahigh density magnetic storage media. It has been demonstrated that the oxide layer of FePt nanoparticles can be removed completely by a 40 s Ar^+ sputtering. Therefore, we can deposit in-situ a thin nonmagnetic layer to prevent from the oxidation of FePt nanoparticles under ambient conditions; moreover, such a nonmagnetic matrix can isolate magnetic grains and avoid intergranular exchange coupling. The latter is a key parameter in limiting media noise that ultimately controls storage area density.

We have demonstrated that a hexagonal order array of magnetic FePt nanoparticles could be fabricated using a diblock polymer micellar method combination with plasma treatment. The sequence of adding salts has an effect on the composition distribution. The salts added earlier are preferred to occupy the inner part of P2VP blocks, and simultaneously adding Fe and Pt salts is favoured to obtain a uniform composition distribution. After annealing, the ordered structure of nanoparticles is maintained, indicating that the ordered arrays of FePt nanoparticles have an excellent stability against particle agglomeration.

References

[1] Weller D, Moser A, Folks L, Best M E, Lee W, Toney M F, Schwickert M, Thiele J U and Doerner M F 2000 *IEEE Trans. Magn.* **36** 10
[2] Sun S 2006 *Adv. Mater.* **18** 393
[3] Sun S, Murray C B, Weller D, Folks L and Moser A 2000 *Science* **287** 1989
[4] Luo C P, Liou S H, Gao L, Liu Y and Sellmyer D J 2000 *Appl. Phys. Lett.* **77** 2225
[5] Yang T, Ahmad E and Suzuki T 2002 *J Appl. Phys.* **91** 6860
[6] Xu Y, Sun Z G, Qiang Y and Sellmyer D J 2003 *J. Appl. Phys.* **93** 8289
[7] Elkins K E, Vedantam T S, Liu J P, Zeng H, Sun S and Wang Z L 2003 *Nano Lett.* **3** 1647
[8] Sun S, Anders S, Thomson T, Baglin J E E, Toney M F, Hamann H F, Murray C B and Terris B D 2003 *J. Phys. Chem.* B **107** 5419
[9] Dai Z R, Sun S and Wang Z L 2001 *Nano Lett.* **1** 443
[10] Boyen H G, Fauth K, Stahl B, Ziemann P, Kästle G, Weigl F, Banhart F, Hessler M, Schütz G, Gajbhiye N S, Ellrich J, Hahn H, Büttner M, Garnier M G and Oelhafen P 2005 *Adv. Mater.* **17** 574
[11] Pileni M P 1997 *Langmuir* **13** 3266
[12] Spatz J P, Mössmer S, Hartmann C, Möller M, Herzog T, Krieger M, Boyen H G, Ziemann P and Kabius B 2000 *Langmuir* **16** 407
[13] Kästle G, Boyen H G, Weigl F, Lengl G, Herzog T, Ziemann P, Riethmüller S, Mayer O, Hartmann C, Spatz J P, Möller M, Ozawa M, Banhart F, Garnier M G and Oelhafen P 2003 *Adv. Funct. Mater.* **13** 853
[14] Yun S H, Sohn B H, Jung J C, Zin W C, Lee J K and Song O 2005 *Langmuir* **21** 6548
[15] Boyen H G, Kästle G, Zürn K, Herzog T, Weigl F, Ziemann P, Mayer O, Jerome C, Möller M, Spatz J P, Garnier M G and Oelhafen P 2003 *Adv. Funct. Mater.* **13** 359
[16] Ethirajan A, Wiedwald U, Boyen H G, Kern B, Han L, Klimmer A, Weigl F, Kästle G, Ziemann P, Fauth K, Cai J, Behm R, Romanyuk A, Oelhafen P, Walther P, Biskupek J and Kaiser U 2007 *Adv. Mater.* **19** 406
[17] Fuggle J C and Martensson N 1980 *J. Electron Spectrosc. Relat. Phenom.* **21** 275
[18] Kodama H, Momose S, Sugimoto T, Uzumaki T and Tanaka A 2005 *IEEE Trans. Magn.* **41** 665